

Impact of non-uniform beam filling on spaceborne cloud and precipitation radar retrieval algorithms

Simone Tanelli^a, Gian Franco Sacco^a, Stephen L. Durden^a, Ziad S. Haddad^a

^a Jet Propulsion Laboratory, California Institute of Technology, Pasadena, CA 91109

ABSTRACT

In this presentation we will discuss the performance of classification and retrieval algorithms for spaceborne cloud and precipitation radars such as the Global Precipitation Measurement mission [1] Dual-frequency Precipitation Radar (GPM/DPR) [2], and notional radar for the Aerosol/Clouds/Ecosystem (ACE) [1] mission and related concepts. Spaceborne radar measurements are simulated either from Airborne Precipitation Radar 2nd Generation (APR-2, [3]) observations, or from atmospheric model outputs via instrument simulators contained in the NASA Earth Observing Systems Simulators Suite (NEOS³). Both methods account for the three dimensional nature of the scattering field at resolutions smaller than that of the spaceborne radar under consideration. We will focus on the impact of non-homogeneities of the field of hydrometeors within the beam. We will discuss also the performance of methods to identify and mitigate such conditions, and the resulting improvements in retrieval accuracy. The classification and retrieval algorithms analyzed in this study are those derived from APR-2's Suite of Processing and Retrieval Algorithms (ASPRA); here generalized to operate on an arbitrary set of radar configuration parameters to study the expected performance of spaceborne cloud and precipitation radars. The presentation will highlight which findings extend to other algorithm families and which ones do not.

Keywords: GPM, ACE, NUBF, SRT.

1. INTRODUCTION

The fundamental principle behind multi-frequency radar retrievals of cloud and precipitation properties is that of exploiting the difference in backscattering and extinction signatures of the hydrometeors among the various frequencies. On one hand we rely upon the onset of resonances in the so-called Mie regime for particle sizes that are not much smaller than each wavelength, and on the other hand we rely upon the extinction (or attenuation) signature that grows rapidly with increasing frequency and is more closely associated to the precipitation rate (at least in rainfall). A reader is directed to a wealth of publications (see. e.g., [4] through [8] and references cited therein) that address this matter in detail. Three specific points are central to this work: a) almost all retrieval algorithms benefit of independent information on the Path Integrated Attenuation (PIA, in this document we always indicate the 2-way attenuation as PIA) to constrain or validate the ambiguous retrieval process; b) over ocean one of the most mature approaches is that of the Surface Reference Technique (see e.g., [5] and [9]) where the PIA is derived by subtracting the observed surface Normalized Radar Cross Section (NRCS) from the expected NRCS that one would have observed in absence of precipitation; c) the importance of the PIA information grows together with the magnitude of the PIA, and therefore it is in general more and more important as higher and higher frequencies are adopted.

No matter whether an algorithm makes use of the PIA as input or not, it will rely upon prescribed mapping between the backscattering properties of the hydrometeor distribution and the corresponding specific attenuation. Such mapping is often implemented as Look-Up-Tables (LUT) or power laws that associate a non-attenuated reflectivity factor Z_e to a specific attenuation k for each frequency given a certain Particle Size Distribution (PSD) for assumed particle types. While the relations between Z_e and k at various frequencies are far from being unique (hence the ambiguities in the retrievals), it does cover a certain search domain (that is a portion of the entire hypercube of the observable quantities). When more and more frequencies are employed simultaneously, the fractional size of the search domain decreases progressively as more and more constraints reduce the level of ambiguity. If we now assume that the footprint of the radar is not entirely populated by a homogeneous (in the direction orthogonal to the look direction) distribution of hydrometeors the mapping described above is not valid anymore. This situation is commonly referred to as Non-Uniform Beam Filling (NUBF), and its impact was recognized and described early on before the launch of the Tropical

Rain Measurement Mission (TRMM) [10] and characterized in subsequent studies (see e.g., [12]). Several approaches were tested and implemented to correct for it [11]. However, both the resulting errors and the capability to mitigate them were reduced in TRMM because its Precipitation Radar (PR) is a single-frequency Ku-band radar [13]. In other words, on one hand we have that since Ku-band specific attenuation is only approximately $k = 0.02 R^{1.1}$ where k is in dB/km and R is in mm/hr, attenuation plays an important role in TRMM only in strong rain events, but on the other hand there is little information in TRMM that allows to detect NUBF and correct for its effects. All the correction algorithms had to rely upon statistical assumptions derived from other (non-collocated) observations or climatology.

The GPM/DPR will provide collocated Ku- and Ka-band measurements of reflectivity, and the radar planned for the ACE mission will provide collocated Ka- and W-band measurements. In both cases we can expect an increase in the NUBF effects because of the higher specific attenuations, but also the means to detect it directly and to a certain extent correct it because of their multi-frequency nature.

In this paper we first summarize the conceptual impact of NUBF on multi frequency profiles of reflectivity, then provide the basis for its direct detection by a multi-frequency radar system pointing close to nadir, and illustrate expected occurrence based on experimental data. Finally we show some preliminary results of a new NUBF-compensating approach applied to simulated GPM and ACE measurements.

2. CONCEPTUAL DESCRIPTION OF NUBF EFFECT ON MULTI-FREQUENCY RADAR PROFILES

As done in [10] we will adopt a simplified scenario to illustrate the impact of NUBF on multi-frequency radar profiles. Let us assume for sake of simplicity that a multi-frequency radar pointing exactly at geodetic nadir (i.e., orthogonal to the local tangent of the Earth's ellipsoid) has all beams perfectly matched and operating simultaneously. Let us also assume that it is observing a simplified stratiform rain scene, that is a scene where an upper portion of low density ice particles introduces negligible attenuation at all frequencies used, and where a lower portion of rain does introduce some attenuation. We also assume that the rainfall is homogeneous vertically, but not homogeneous horizontally. We refer to this first model as VH-NUBF (Vertically Homogeneous NUBF).

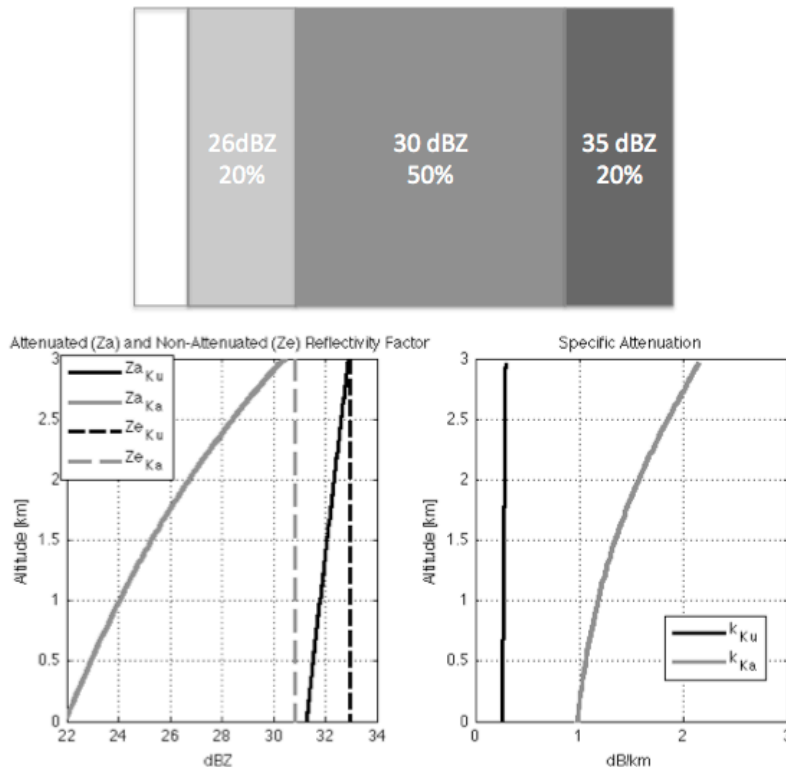


Figure 1: Simplified diagram of NUBF effect on multi-frequency profiles of radar reflectivity.

Figure 1 shows on the upper panel a graphic representation of a scene where it is assumed for sake of discussion that the footprint can be divided in 4 portions, each with a vertically homogeneous rain layer. Each portion is described by a fractional amount (or Probability P), a mass concentration (M), and mean particle diameter (D). In the example depicted here we assume $P = [0.1 \ 0.2 \ 0.5 \ 0.2]$, $M = [0 \ 0.1 \ 0.3 \ 1]$ g/m^3 , $D = [0 \ 1 \ 1 \ 1.3]$ mm, respectively. According to a LUT calculated with T-matrix theory, assuming gamma distribution DSD and oblate raindrops, each of the 4 portions results in the non attenuated reflectivity factors $Ze = [-Inf \ 28.0233 \ 32.0944 \ 37.1832]$ dBZ at Ku band and $Ze = [-Inf \ 25.8929 \ 29.9640 \ 35.0528]$ at Ka band, and the specific attenuations $k = [0 \ 0.0554 \ 0.1414 \ 0.4363]$ dB/km at Ku-band and $k = [0 \ 0.4202 \ 1.0729 \ 3.3114]$ dB/km at Ka-band. It could be viewed as a footprint where a cumulus congestus

was observed, with a glancing hit to its convective core and a small portion of the footprint falling in the clear air surrounding it. When all the 4 portions are accounted for within the footprint, the resulting observed profiles of reflectivity are shown on the right. The first thing that one can notice is that the Ka-band profile of reflectivity does not have a constant slope (this is actually true also for the Ku-band, but the magnitude of that signal is one order of magnitude smaller). However, the ‘truth’ average Ze profile is indeed and obviously constant (since all the rain is vertically homogeneous), in fact the apparent specific attenuation backed out of the slope is shown to vary all the way from about 1.0 dB/km at the bottom to more than 2 dB/km at the top, a factor of more than 2. This can be explained intuitively by considering that the portion that ‘contributes the most’ to the observed reflectivity at the top of the column is also the one that is attenuated the fastest, as its contribution drops below the next-strongest rain column that second column’s specific attenuation starts to dominate the shape, and so forth.

These effects were already discussed in e.g., [10], [12], [14] but focusing only on their effects at the top and bottom of the rain layer, or on single-frequency profiles. Since we are now interested in dual-frequency profiling algorithms capable of retrieving not only precipitation rates but also mean drop diameters, the effect described above is sufficient to introduce a significant issue for any standard algorithm that, one way or another, assumes that any particular homogeneous DSD will always result in the same quadruplet of Ze and k. Depending on the constraining logic of the specific algorithm, a profile like this one can introduce conflicting observational constraints that push the retrieval outside of the permissible search domain. Certain algorithms will simply fail to converge; some others may relax to solutions that are affected by significant additional error, depending on the gravity of NUBF. This issue is further compounded by the fact that the resulting shape (i.e., a decreasing slope as we approach the surface) is very similar to the typical signature of multiple scattering that can be expected in convection (note: in this simple simulation there is no multiple scattering involved).

The second key effect that was observed is that the effect of VH-NUBF on the Surface Reference is quite different from that on the last rainfall range bin above the surface. This is due to the fact that the non-attenuated reflected power from the surface can be assumed constant across the footprint, while that from the last rainfall bin is distributed according to the four portions: as result, the apparent attenuation of the surface is in general less or equal than the apparent attenuation at the last rain bin. The difference is proportional to the amount of NUBF. In the example shown in figure 1 the Ku- and Ka-band profiles of reflectivity have been attenuated approximately 2 and 9 dB (2-way) respectively, but the surface reference under the same conditions is attenuated 2-way only 1.1 and 5.6 dB, respectively. Once again, if one were to apply a standard multi-frequency SRT method to the PIA so derived, it would introduce self-contradicting constraints to the algorithm.

This example was drawn with the GPM/DPR Ku-/Ka-band channels in mind. Very similar considerations apply to any other combination of frequencies involving attenuated frequencies. The magnitude of the impact increases with the operating frequency. Smaller footprints can reduce the probability of occurrence, but do not alter the magnitude when equivalent levels of NUBF occur within the footprint. It follows that in the case of the ACE radar (Ka-/W-band) the impact of NUBF is larger than for GPM, but on the other hand the smaller footprint (2 km requirement at Ka-band, 1 km requirement at W-band) tends to reduce its occurrence.

Before we discuss how often we estimate that this will be a significant issue, or how to take advantage of its observable features to detect it with multi-frequency spaceborne radars, it is useful to briefly introduce a second type NUBF: the 3D-NUBF where vertical homogeneity does not occur. It will be shown how this second type of NUBF represents a more challenging situation, whose effects can be however often mitigated through a VH-NUBF approximation.

3. OCCURRENCE AND EFFECTS

In order to obtain a preliminary indication of how often the GPM DPR will be affected by NUBF we processed the data from the Airborne Precipitation Radar 2nd Generation (APR-2) from the GRIP and Wakasa Bay experiment in a similar fashion as in [14] to obtain profiles and PIA estimates as they would have been observed by GPM DPR pointed at nadir. One difference in the approach is that instead of performing 2-D integration (i.e., along-track and vertical), we now perform 3-D integration: the APR-2 estimates of PIA are combined across the swath (and in the along track direction) assuming a constant NRCS background within a footprint to generate the GPM-observed attenuated NRCS. All NRCS and reflectivity contributions are combined according to a Gaussian distribution to simulate the main beam of DPR.

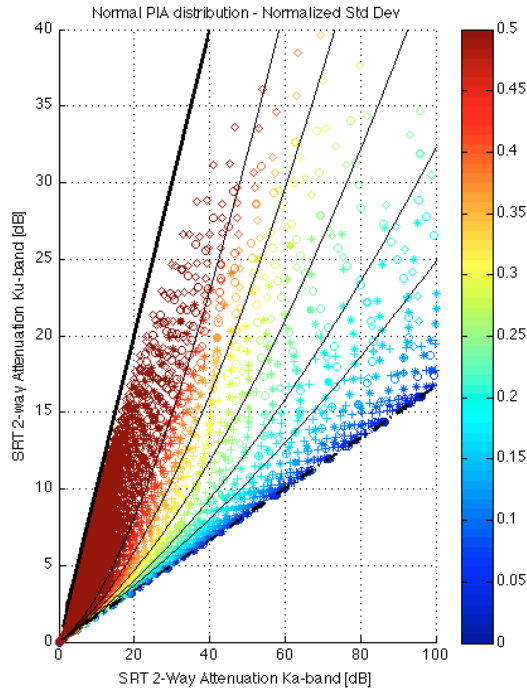


Figure 2: Surface attenuation observable by GPM/DPR under various VH-NUBF conditions modeled with a Gaussian distribution. The colorscale indicates the Ka-band σ_{PIA} normalized by μ_{PIA} .

As shown in [10], [12] and [14] a link exists between the standard deviation of PIA (σ_{PIA}) within the footprint, and the resulting errors incurred by simplified retrieval algorithms because of NUBF. Such quantity can therefore be used as quantitative indicator of NUBF. In the single-frequency situations, efforts were made to estimate σ_{PIA} (or an equivalent parameter) within the footprint by applying scaling considerations and empirical evidence to the observed σ_{PIA} observed at the inter-footprint scale. Unfortunately the residual uncertainties of this process of estimation resulted in somewhat erratic results in TRMM and therefore the NUBF-correction has been disabled in the latest releases [13].

A second simple model for VH-NUBF assumes a Gaussian distribution of PIA centered on μ_{PIA} and with σ_{PIA} standard deviation. The distribution is obviously limited to positive values, with zero assuming the probability of the integral portion of Gaussian distribution that falls at or below zero. This is not an unreasonable model given the so called intermittent nature of the rain process. An ensemble of simulations spanning the range of realistic PIA distributions results in the diagram in Figure 2. The color scale indicates the normalized standard deviation within the footprint ($\sigma_N = \sigma_{PIA} / \mu_{PIA}$). In the x-y space of the NRCS attenuation at Ku- and Ka-band, PIA_{SRKu} and PIA_{SRKa} two quantities that

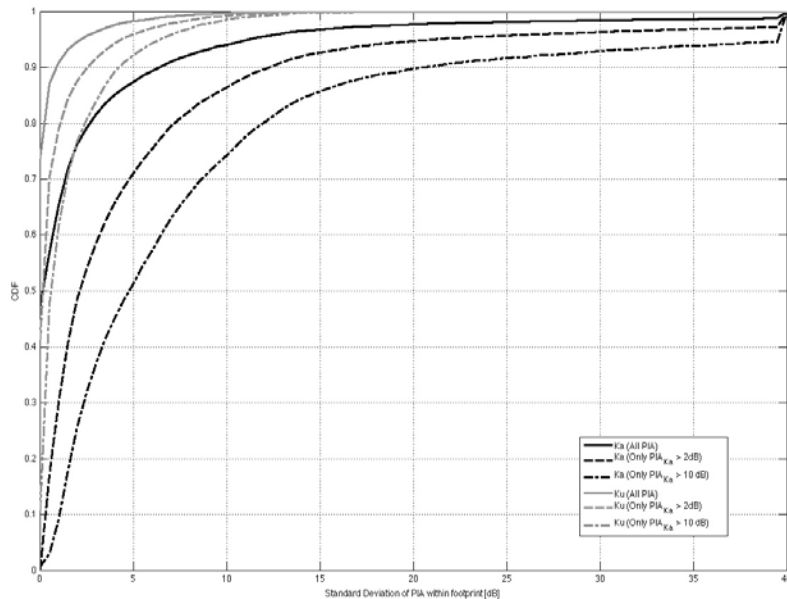


Figure 3: cumulative distribution function of σ_{PIA} within one GPM/DPR footprint calculated from the APR-2 observations during the NASA Genesis and Rapid Intensification Processes (GRIP) experiment (Tropical Atlantic, Gulf of Mexico and Caribbean, August and September 2010).

will be estimated by GPM/DPR simultaneously) the stratification by the degree of NUBF is evident: all profiles with minimal NUBF (indicated by the low values of σ_N) lie along the 6:1 line where the ratio between k_{Ka} and k_{Ku} is generally expected to fall (dash black). As σ_N grows, the points fall closer and closer to the 1:1 line which is expected asymptotically when all that matters is how much of the surface is visible through non-attenuating columns and how much is hidden behind extreme attenuation. With a dual-frequency radar we can therefore deduce the degree of NUBF just out of estimates of PIA obtained from surface reference. While the various sources of departure from this simple model are not depicted here, they contribute in general only a fraction to a few dB each (e.g., uncertainty in the estimation of the reference NRCS, variability in the k_{Ka}/k_{Ku} ratio, gaseous attenuation).

Figure 3 shows the cumulative distribution function (cdf) of standard deviation of PIA inside one DPR footprint at Ka-band. We define for ease of interpretation a threshold at 2dB to separate uniform conditions from non-uniform conditions, and a second threshold at 10dB to separate moderate NUBF from extreme NUBF. For reference, the example discussed in section 2 has a standard deviation of ~ 6.5 dB.

The GRIP dataset indicates that in tropical conditions we could expect more than 80% of all profiles not to be affected significantly by NUBF at Ka band, however, if only the profiles where a non-negligible Ka-band attenuation is observed are considered, that fraction drops to about 55%. If we then consider only profiles with significant attenuation (i.e., larger than 10 dB) then only less than 40% of those profiles can be safely treated under the uniform beam filling assumption. Furthermore, of said profiles almost 25% are expected to fall in the extreme NUBF category. Under the same conditions the impact of NUBF at Ku-band is, as expected, significantly less important (grey curves in Figure 3). Clearly the tropics are the region where the impact of NUBF is expected to be the largest in general, but it should be expected also that extreme convection over land outside of the tropics or some instances of orographic precipitation may be affected by significant NUBF. In both cases, there are other significant sources of uncertainty due to multiple scattering, mixed phase particles, and hail that are not addressed in this paper.

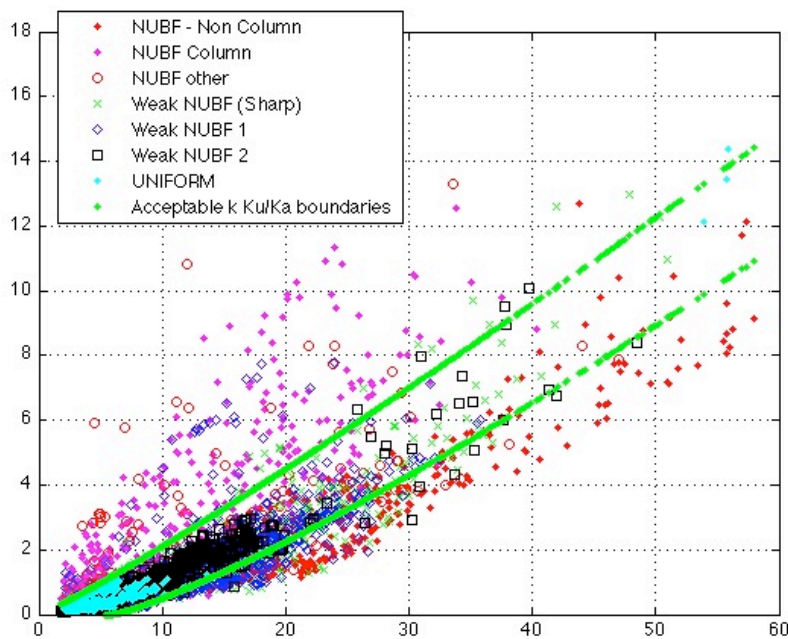


Figure 4: Distribution of GPM PIA_{SR} at Ku- and Ka-band (y and x axes, respectively) simulated from the APR-2 dataset. The categories shown in the legend were determined through analysis of the APR-2 data at their native resolution (see text for details). The two green curves delimit the region where one should expect the PIA_{SR} pair to fall in case of uniform rain. We refer to the portion to the right of it as the 3D-NUBF region, and to the one to the left as the VH-NUBF region (with the degree of NUBF increasing from the right to the left).

The same APR-2 dataset was used to verify whether the simple model adopted to generate Figure 2 was capturing a realistic link between the observed pair (PIA_{SRKu}, PIA_{SRKa}) and the degree of NUBF within the footprint. Figure 4 shows a similar diagram as Figure 2, but this time the (PIA_{SRKu}, PIA_{SRKa}) values are derived from simulating the GPM/DPR footprint out of the APR-2 data, and each point was catalogued based on the effective distribution of reflectivity and PIA within the footprint. It can be seen that 4 categories fall in the general region dictated by documented k relationship between Ku- and Ka-band in rain (hereinafter referred to as the self-consistent region): the uniform beams (i.e., where $\sigma_{PIA} < THR$), and three types of weak NUBF (i.e., where some degree of NUBF is present, but the magnitudes of the attenuations and their variability are such that very small impact on retrievals can be expected). A fifth category is that of moderate NUBF-Column, that is a situation similar to VH-NUBF but with some minor variability in the vertical: in this case the samples fall in the region predicted by Figure 2, and follow approximately the shown dependency to

σ_{PIA}). The last two categories are the least treatable types of NUBF: the first is the ‘Non-Column NUBF’, a truly 3D-NUBF situation where the variability in the vertical is of the same magnitude as that in the horizontal (these conditions were verified to correspond generally to slanted rain shafts resulting from wind shear by visual inspection of a sub sample). It is interesting to note that many of these profiles fall in the region to the right of the self-consistent region, outside of the range predicted by Figure 2, which is in fact based on the VH-NUBF. Some of them though fall inside the self-consistent region or in the VH-NUBF region to the left. The final category of the ‘NUBF Other’ includes profiles that did not match any of the selection criteria of the above categories; most of these profiles fall in the VH-NUBF

region, including especially the extreme region closest to the 1:1 line. A visual depiction from real data of three of these categories is shown in Figure 5.

For profiles that fall within the VH-NUBF region we can therefore use Figures 2 and 3 in conjunction with the results shown in [14] to obtain a first order assessment of the impact of NUBF at Ku- and Ka-band on retrieved rainfall rates at the surface and at the top of the rain layer. An algorithm has been developed to provide an estimation of NUBF for cases where $0.15 \leq \sigma_N \leq 0.5$. For cases closer to the 1:1 line (i.e., $\sigma_N > 0.5$), the uncertainty associated with this estimation process is expected to result in residual uncertainties as large as the correction itself (or more) for the near-surface correction. These cases are therefore only flagged as extreme NUBF and no correction has been developed yet.

Also, no correction is applied to the cases falling inside the self-consistent region since in the majority of those cases no correction is necessary. No correction has been developed yet for cases falling in the 3D-NUBF region, however they are detected and flagged. For cases in the extreme-NUBF or in the 3D-NUBF regions, a first order recommendation (until an algorithm is developed) is to avoid use of the multi-frequency approaches and revert to a single-frequency approach

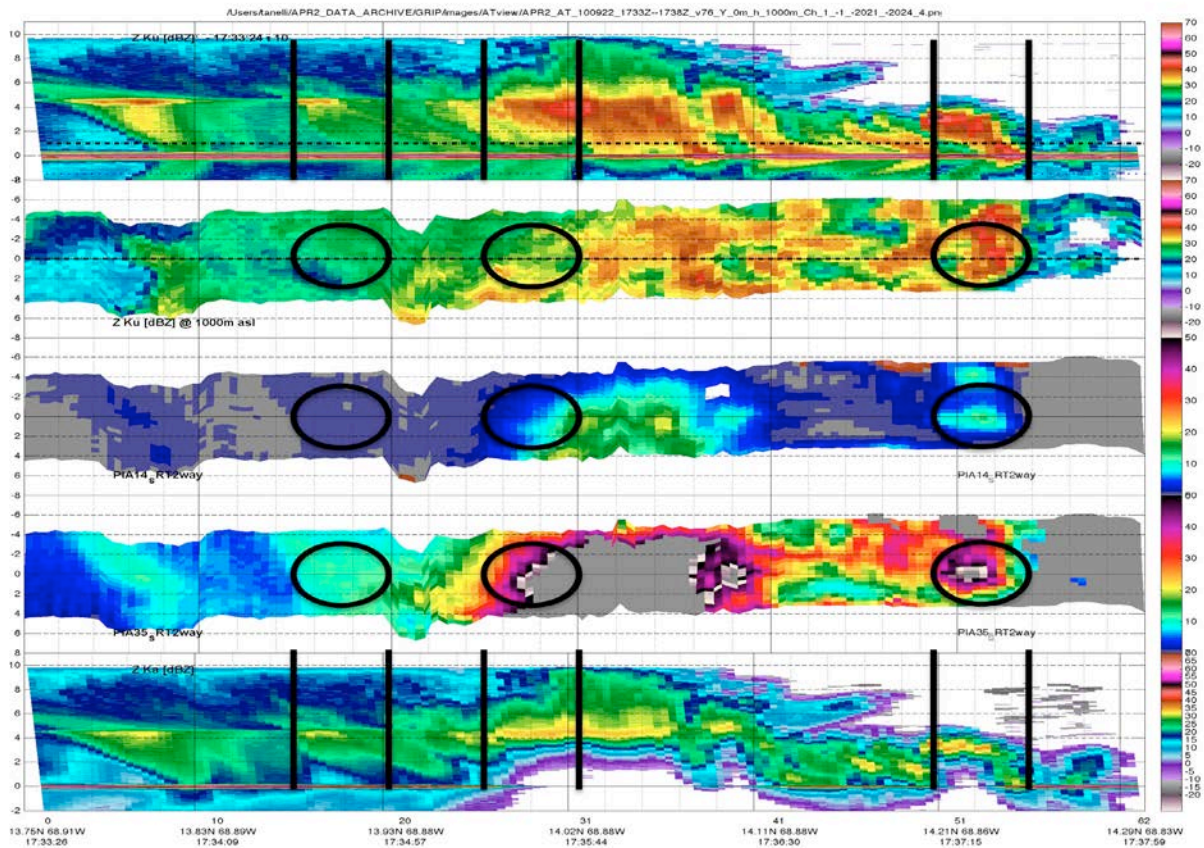


Figure 5: example of three types of NUBF conditions from the GRIP APR-2 dataset. Top to bottom: vertical curtain of APR-2 Za_{Ku} , horizontal section at 1 km altitude of Za_{Ku} , swath of $PIA_{SR_{Ku}}$, swath of $PIA_{SR_{Ka}}$ (note: the grey section in the rainy regions indicates that the PIA exceeded the dynamic range of 60 dB), vertical curtain of APR-2 Za_{Ka} . Three GPM DPR footprints (3dB) are shown: the first observes a region with 3D-NUBF but of such small magnitude that it results in a nearly homogeneous PIA field, no mitigation is necessary; the second falls in a stratiform region of heavy precipitation with significant gradients in PIA within the footprint, this is a heavy NUBF case almost vertically homogeneous that can be mitigated; the third footprint is a case of a small slanted shallow convective cell that results in 3D-NUBF and whose PIA_{SR} at Ku and Ka band fall in the 3D-NUBF region in the diagram in Figure 4, no correction is activated, but the profile is flagged.

relying solely on the lowest available frequency which is impacted less by NUBF. The resulting retrievals will surely be of lower accuracy as the multi-frequency ones acquired where NUBF is not present, but they will at least converge to a well understood set of assumptions and not be affected by the erratic performance similar to the one observed in TRMM with the original NUBF-correction [13].

The impact of NUBF conditions on multi-frequency profiling of rain and the potential of NUBF corrections is illustrated in Figure 6. For this example, similar to the one shown in Figure 1, we assume $P = [0.1 \ 0.3 \ 0.4 \ 0.2]$, $M = [0 \ 0.4 \ 0.8 \ 2] \text{ g/m}^3$, and $D = [0 \ 1 \ 1 \ 1.3] \text{ mm}$. In these conditions the GPM-observed PIA_{SR} is of 2.2dB at Ku-band and 8.6 dB at Ka band, while the standard deviation of PIA within the footprint is 2 and 15 dB, respectively. One can notice immediately that in this profile, where Z_e is assumed constant in height, the Ka-band at the surface is attenuated by more than 15 dB while the PIA_{SR} is only 8.6 dB. Application of a the standard APR-2 retrieval algorithm (a fully Bayesian implementation of the combined top-down and SRT method) in this case does deliver a retrieved profile of attenuated reflectivity Z_a that is not too dissimilar from the observed one (solid curves in the top left panel). However one can immediately notice that the corresponding non-attenuated reflectivity factors Z_e (dashed lines) do not capture the true nature of the profile (they are both not constant in height, and they diverge from truth as one approaches the surface, by as much as 7dB at the bottom of the profile. Furthermore, it is also their ratio (the dual-wavelength ratio, DWR) that changes significantly along the profile. As result, the mean particle size is generally centered around the truth value, but it does depart by more than 20% at the surface, and the expected anti-correlated behavior is observed in total liquid estimates which approach the truth at the top of this profile, but are grossly underestimated at the near surface (by more than a factor 5).

We have implemented a NUBF-estimation algorithm inside the APR-2 based solely on the quantities observable by the GPM-DPR. While this estimation process is prone to uncertainties (proportional to the degree of NUBF being corrected) it did result generally in improved results. The results of the APR-2 retrieval so upgraded, applied to the same profile are shown in the lower panels of figure 6. One can notice that the retrieved Z_a are of no better accuracy of the ones retrieved

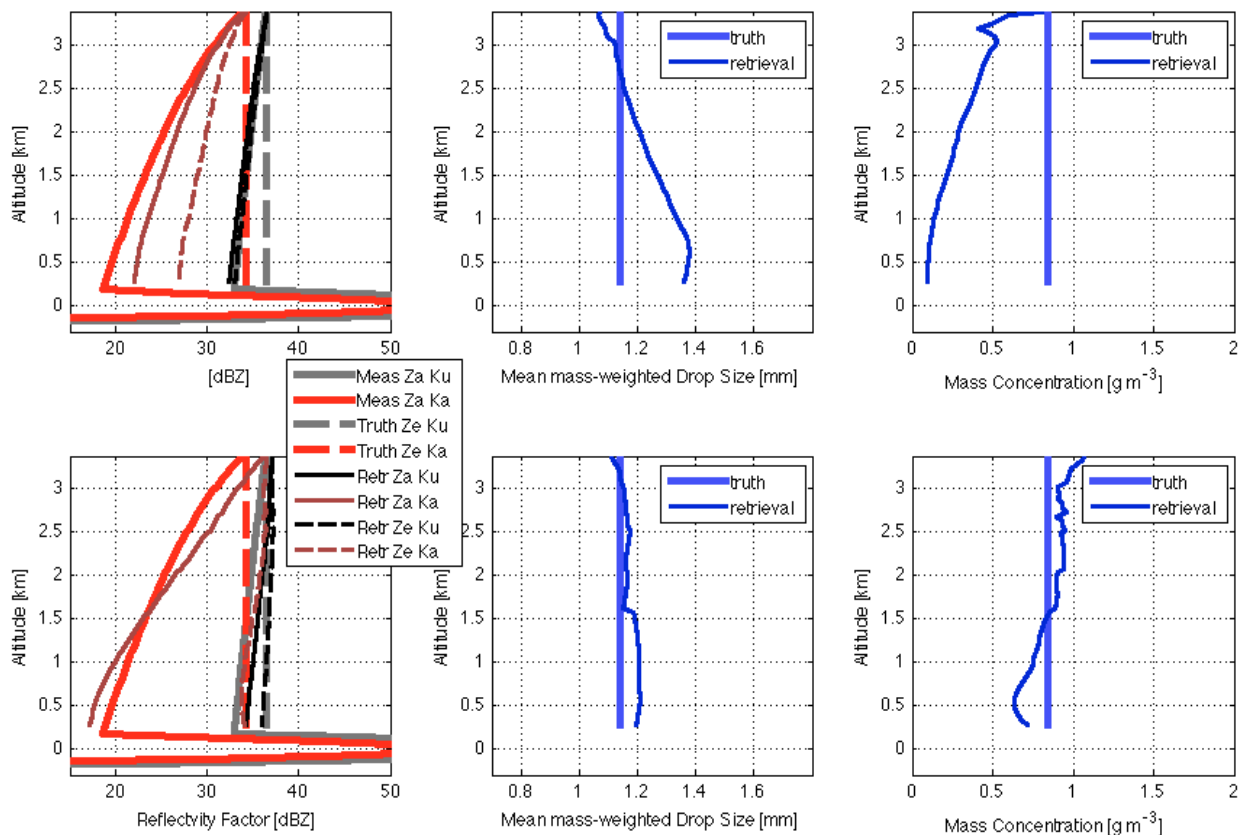


Figure 6: Example of Ku-/Ka-band retrievals obtained by two versions of the APR-2 retrieval algorithm applied to a profile affected by NUBF (see text for details). Top panels show the results of the standard algorithm (with no NUBF estimation) and the lower panels show the results of the upgraded algorithm (with NUBF estimation).

with the standard algorithm, however all the underlying quantities (Z_e , mean particle diameter and mass concentration) are clearly much closer to the truth.

While the impact of NUBF varies significantly from case to case, and depending on which multi-frequency profiling algorithm is adopted, the effects shown in Figure 6 are quite representative of the nature of the problem. In weaker NUBF conditions the effects decrease rapidly and converge to the standard retrievals, in stronger or less vertically homogeneous conditions they can result in completely incorrect results or even in failures to converge to a solution. The same algorithm has been applied also to Ka-/W-band profiles, as well as Ku-/Ka-/W-band profiles: while the impact of NUBF from various scenarios varies greatly depending on the frequencies and the footprint sizes, the general behavior shown in this paper is generally preserved.

4. SUMMARY AND CONCLUSIONS

We have illustrated the nature of the impact of Non-Uniform Beam Filling on multi-frequency radar retrievals of profiles of cloud and precipitation, and provided a preliminary measure of their expected occurrence for the GPM DPR. Impact of NUBF on retrievals ranges from negligible to unacceptable and is expected to be all the more relevant for higher frequency measurements. A simple NUBF-estimation method based solely on the observable quantities has been implemented and tested with promising results. The same algorithm was applied also to the ACE radar frequencies (Ka-/W-band).

ACKNOWLEDGEMENTS

The research described in this paper was carried out at the Jet Propulsion Laboratory, California Institute of Technology, under contract with the National Aeronautics and Space Administration.

REFERENCES

- [1] NRC (Nat. Research Council), "Earth Science and Applications from Space: National Imperatives for the Next Decade and Beyond," 2007
- [2] Senbokuya, Y., et al., "Development of the spaceborne dual-frequency precipitation radar for the Global Precipitation Measurement mission," in Proc. IGARSS, 3566–3569 (2004).
- [3] Sadowy, G. A., A. C. Berkun, W. Chun, E. Im, and S. L. Durden, 2003: Development of an advanced airborne precipitation radar. *Microwave J.*, **46** (1), 84-98.
- [4] Meneghini, R., and T. Kozu, 1990: Spaceborne Weather Radar. Artech House, 201 pp.
- [5] Meneghini, R., H. Kumagai, J. R. Wang, T. Iguchi, and T. Kozu, 1997: Microphysical retrievals over stratiform rain using measurements from an airborne dual-wavelength radar-radiometer. *IEEE Trans. Geosci. Remote Sens.*, **35**, 487-506.
- [6] Haddad, Z. S., E. Im, and S. L. Durden, 1995: Intrinsic ambiguities in the retrieval of rain rates from radar returns at attenuating wavelengths. *J. Appl. Meteor.*, **34**, 2667-2679.
- [7] Mardiana R., Iguchi, T.; Takahashi, N., 2004; A dual-frequency rain profiling method without the use of a surface reference technique, *IEEE Trans. Geosc. and Rem. Sens.*, **42**, 2214 – 2225.
- [8] Grecu, M., L. Tian, W. S. Olson, and S. Tanelli, 2011: A robust dual-frequency radar profiling algorithm. *J. Appl. Meteor. and Climatol.*, **50**, 1543-1557
- [9] Meneghini, R.; L. Liao; S. Tanelli, S.L. Durden, 2012: Assessment of the Performance of a Dual-Frequency Surface Reference Technique Over Ocean, *Geoscience and Remote Sensing, IEEE Transactions on*, vol.50, no.8, pp.2968-2977, Aug. 2012. doi: 10.1109/TGRS.2011.2180727
- [10] Nakamura, K., 1991: Biases of rain retrieval algorithms for spaceborne radar caused by nonuniformity of rain. *J. Atmos. Oceanic Technol.*, **8**, 363–373.
- [11] Iguchi, T., 2000: Rain profiling algorithm for the TRMM precipitation radar. *J. Appl. Meteor.*, **39**, 2038-2052.
- [12] Durden S.L., E. Im, Z. S. Haddad, A. Kitiyakara, and F. K. Li, 1998: Effects of nonuniform beam filling on rainfall retrieval for the TRMM precipitation radar. *J. Atmos. Oceanic Technol.*, **15**, 635–646.
- [13] Iguchi, T.; , "Evolution of the rain profiling algorithm for the TRMM Precipitation Radar," *Geoscience and Remote Sensing Symposium (IGARSS)*, 2011 *IEEE International*, pp.1562-1564, 24-29 July 2011 doi: 10.1109/IGARSS.2011.6049368
- [14] S. L. Durden and S. Tanelli, "Predicted effects of nonuniform beam filling on GPM radar data," *IEEE Geosci. Remote Sens. Lett.*, vol. 5, no. 2, pp. 308-310, April 2008